Supporting Information

Anisotropic Picosecond Spin-Photocurrent from Weyl Semimetal WTe_2

Mengji Chen,[†,°] *Kyusup Lee,*[†,°] *Jie Li,*[‡] *Liang Cheng,*[§] *Qisheng Wang,*[†] *Kaiming Cai,*[†] *Elbert E. M. Chia,*[§] *Haixin Chang,*[‡] *and Hyunsoo Yang*[*,†]

† Department of Electrical and Computer Engineering and NUSNNI, National University of Singapore, 117576, Singapore

‡ Center for Joining and Electronic Packaging, State Key Laboratory of Material Processing and Die & Mould Technology, School of Materials Science and Engineering, Huazhong University of Science and Technology, Wuhan 430074, China

§ Division of Physics and Applied Physics, School of Physical and Mathematical Sciences, Nanyang Technological University, 637371, Singapore

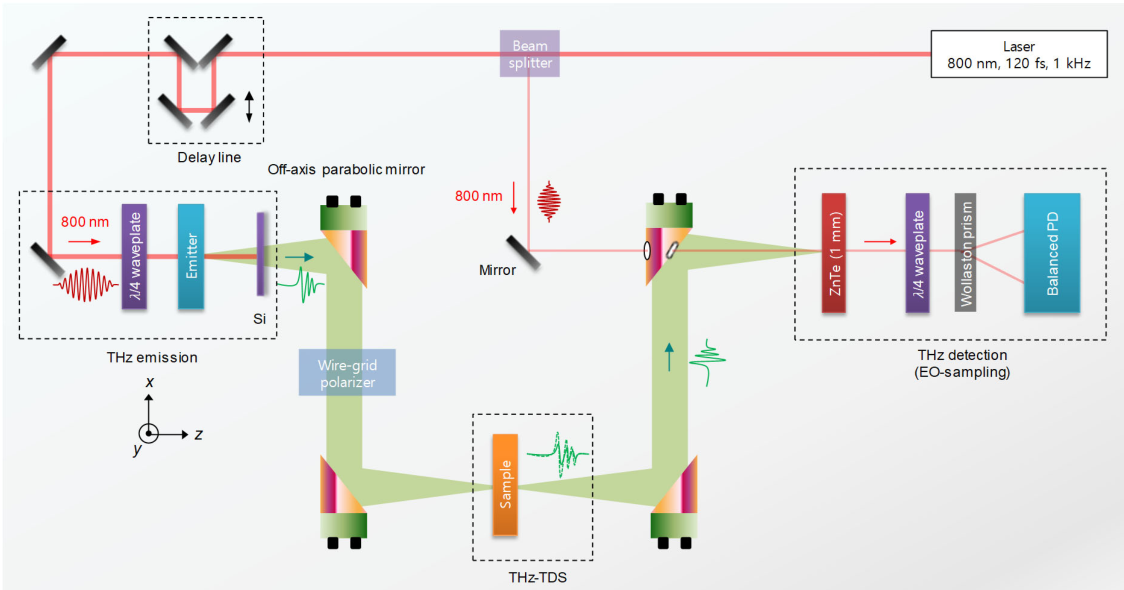

Supporting figure S1. The schematic diagram of the terahertz emission measurement and the time-domain spectroscopy (THz-TDS). The laser beam is divided into the pump and probe lines to excite an emitter and a detector (here, 1-mm thick ZnTe), respectively. For the emission measurement, the 50-nm thick Td-WTe_2 thin film is located at the emitter position in the THz emission site, and the THz-TDS site is empty. The Cartesian axes are defined such that the laser propagates along the *z*-axis and the *x*-axis is horizontally aligned. On the other hand, during the THz-TDS measurement for the conductivity analysis, a 1-mm thick ZnTe is used to emit THz radiation and the Td-WTe_2 film is inserted at the sample position in the THz-TDS site. A typical electro-optic (EO) sampling is used for THz detection in the time domain using a mechanical delay line. The optical pump polarity is controlled by a quarter-wave (λ/4) plate. A wire grid polarizer is used to filter out the THz polarization along the *x*-axis.

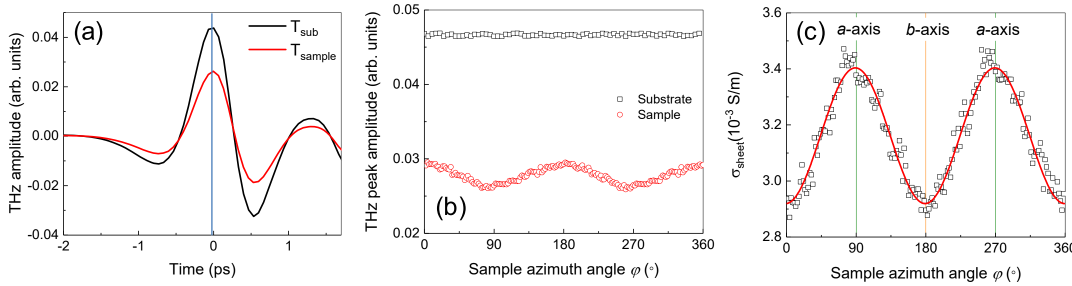

Supporting figure S2. In-plane conductivity analysis extracted by a THz-TDS. (a) The THz waveforms transmitted through the bare substrate and the Td-WTe_2 film. (b) The transmitted THz peak amplitude as a function of the sample azimuth angle. (c) The derived angle-dependent conductivity, which is added as Figure 1c in the main text. The conductivity exhibits two-fold symmetry and is minimized (maximized) along 0° (90°), indicating the crystallographic *b*(*a*)-axis.

It has been known that the conductivity of the Td-WTe_2 film is higher along the *a*-axis than the *b*-axis.[1,2] We thus use an in-plane conductivity to define the in-plane crystallographic axis in Td-WTe_2. We utilize an in-situ all-optical tool to evaluate the conductivity as shown in figure S2. Due to the fact that a THz photon sensitively interacts with intrinsic charge carriers inside medium, THz transmission measurements have been extensively used to quantify the dc conductivity.[3,4]

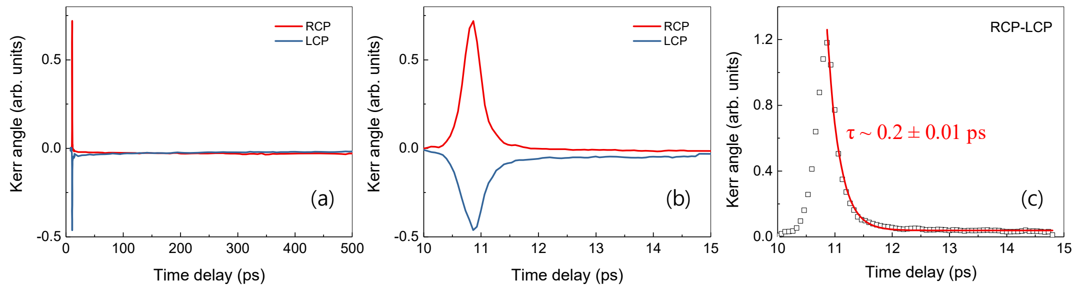

Supporting figure S3. Optical helicity dependent TR-MOKE signal in the bulk Td-WTe_2 (50 nm) with (a) a long scan up to 500 ps and (b) a fine scan up to 15 ps. (c) The subtraction signal (RCP-LCP). The solid red line is an exponential fit with a time constant τ representing a spin lifetime.

It has been noted that thicker WTe_2 exhibits a larger density of states,[4,5] *i.e.*, a larger phase space for both interband and intraband transition, which induces a higher scattering probability during spin relaxation. This, in turn, gives rise to a faster relaxation with a shorter lifetime. Indeed, in this report, the polarity changes with the optical pump helicity such as right and left circular polarization states (RCP and LCP, respectively), which indicates its spin origin. We rule out the charge-carrier contribution by subtracting two signals (RCP-LCP). The rise and decay trends of the RCP-LCP signal within a picosecond represent the sub-picosecond thermalization and energy relaxation processes, respectively, revealing a spin lifetime of 0.2 ± 0.01 ps as shown in figure S3. Moreover, a nanosecond spin-dynamics is not observable in the measured time window up to 500 ps. Hence, the obtained sub-picosecond spin dynamics dominates in generating a picosecond spin-photocurrent in the bulk Td-WTe_2 under ultrashort optical excitation, giving rise to THz radiation.

References in Supporting Information

(1) He, P.; Hsu, C.-H.; Shi, S.; Cai, K.; Wang, J.; Wang, Q.; Eda, G.; Lin, H.; Pereira, V. M.; Yang, H. Nonlinear Magnetotransport Shaped by Fermi Surface Topology and Convexity. *Nat. Commun.* **2019,** *10*, 1290.

(2) Kang, K.; Li, T.; Sohn, E.; Shan, J.; Mak, K. F. Nonlinear Anomalous Hall Effect in Few-Layer WTe_2. *Nat. Mater.* **2019,** *18*, 324-328.

(3) Tielrooij, K. J.; Song, J. C. W.; Jensen, S. A.; Centeno, A.; Pesquera, A.; Zurutuza Elorza, A.; Bonn, M.; Levitov, L. S.; Koppens, F. H. L. Photoexcitation Cascade and Multiple Hot-Carrier Generation in Graphene. *Nat. Phys.* **2013,** *9*, 248-252.

(4) Lee, K.; Li, J.; Cheng, L.; Wang, J.; Kumar, D.; Wang, Q.; Chen, M.; Wu, Y.; Eda, G.; Chia, E. E. M.; Chang, H.; Yang, H. Sub-Picosecond Carrier Dynamics Induced by Efficient Charge Transfer in $MoTe_2$/WTe_2 van der Waals Heterostructures. *ACS Nano* **2019,** *13*, 9587-9594.

(5) Wang, Q.; Li, J.; Besbas, J.; Hsu, C.-H.; Cai, K.; Yang, L.; Cheng, S.; Wu, Y.; Zhang, W.; Wang, K.; Chang, T.-R.; Lin, H.; Chang, H.; Yang, H. Room-Temperature Nanoseconds Spin Relaxation in WTe_2 and $MoTe_2$ Thin Films. *Adv. Sci.* **2018,** *5*, 1700912.